

## Application of a Depositional *Facies* Model to an Acid Mine Drainage Site<sup>∇†</sup>

Juliana F. Brown,<sup>1</sup> Daniel S. Jones,<sup>2</sup> Daniel B. Mills,<sup>2</sup> Jennifer L. Macalady,<sup>2</sup> and William D. Burgos<sup>1\*</sup>

*Department of Civil and Environmental Engineering, The Pennsylvania State University, University Park, Pennsylvania,<sup>1</sup> and Department of Geosciences, The Pennsylvania State University, University Park, Pennsylvania<sup>2</sup>*

Received 29 June 2010/Accepted 15 November 2010

**Lower Red Eyes is an acid mine drainage site in Pennsylvania where low-pH Fe(II) oxidation has created a large, terraced iron mound downstream of an anoxic, acidic, metal-rich spring. Aqueous chemistry, mineral precipitates, microbial communities, and laboratory-based Fe(II) oxidation rates for this site were analyzed in the context of a depositional *facies* model. Depositional *facies* were defined as pools, terraces, or microterraces based on cm-scale sediment morphology, irrespective of the distance downstream from the spring. The sediments were composed entirely of Fe precipitates and cemented organic matter. The Fe precipitates were identified as schwertmannite at all locations, regardless of *facies*. Microbial composition was studied with fluorescence *in situ* hybridization (FISH) and transitioned from a microaerophilic, *Euglena*-dominated community at the spring, to a *Betaproteobacteria* (primarily *Ferrovum* spp.)-dominated community at the upstream end of the iron mound, to a *Gammaproteobacteria* (primarily *Acidithiobacillus*)-dominated community at the downstream end of the iron mound. Microbial community structure was more strongly correlated with pH and geochemical conditions than depositional *facies*. Intact pieces of terrace and pool sediments from upstream and downstream locations were used in flowthrough laboratory reactors to measure the rate and extent of low-pH Fe(II) oxidation. No change in Fe(II) concentration was observed with <sup>60</sup>Co-irradiated sediments or with no-sediment controls, indicating that abiotic Fe(II) oxidation was negligible. Upstream sediments attained lower effluent Fe(II) concentrations compared to downstream sediments, regardless of depositional *facies*.**

Sedimentary geologists designate depositional *facies* to differentiate among sediments deposited under specific physical, hydrological, geochemical, and biological conditions (27). Although typically applied to large-scale systems such as terrestrial fluvial or marine carbonate formations, depositional *facies* models are inherently applicable at any scale. Fouke et al. (10, 11) developed a depositional *facies* model for travertine deposition at Angel Terrace (Mammoth Hot Springs, Yellowstone National Park [YNP]), where the exposure of high-temperature, CO<sub>2</sub>-rich springwaters to atmospheric conditions creates extreme geochemical gradients over just a few meters. The Angel Terrace study (10) was the first to incorporate and quantify differences among microbial communities and processes in the context of a depositional *facies* model. Microbial communities, mineral compositions, sediment structures (cm scale), and crystal morphologies (μm scale) were identified for each depositional *facies* (10, 11). Sediment morphologies similar to those found at Angel Terrace can be observed at acid mine drainage (AMD) sites worldwide. Terraced iron formations (TIF) at AMD sites such as the Tintillo River in Huelva, Spain, have previously been compared to travertine deposits at hot springs (9).

Similar to Angel Terrace, sediment deposition at the Lower Red Eyes AMD site is characterized by a large mineral precipitate mound (Fig. 1b), across which emerging springwater flows. However, geochemical gradients at Angel Terrace and

Lower Red Eyes are strongly contrasting. The temperature of the water at Angel Terrace decreases from 73.2°C at the spring to 28.0°C within 5 m downstream (10), while the spring at Lower Red Eyes emerges at approximately 9°C and increases to between 13.5 and 28°C by 120 m downstream, depending on seasonal variations. The pH at Angel Terrace increases downstream from pH 6.0 to 8.0 as a result of CO<sub>2</sub> degassing (10), while the pH at Lower Red Eyes decreases downstream from pH 4.0 to 2.4 as a result of Fe(III) hydrolysis and precipitation. At Angel Terrace, the depositional structures are composed of carbonate minerals, while similar structures at Lower Red Eyes consist of Fe(III) minerals precipitated among organic matter.

Based on the physical similarities at Angel Terrace and Lower Red Eyes, we hypothesized that a depositional *facies* model could be developed for low-pH, Fe(II)-oxidizing, Fe-depositing AMD sites. The application of such a model would imply that a specific depositional environment, such as a terrace or pool, would be an important predictor of Fe(II) oxidation and Fe removal rates. Furthermore, the development and application of an AMD depositional *facies* model could be a useful tool to identify optimal conditions (microbial community structure, aqueous chemistry, geomorphology, and hydrodynamic characteristics) for low-pH Fe(II) oxidation in passive AMD treatment systems.

### MATERIALS AND METHODS

**Field sampling.** Lower Red Eyes is a low-flow (<1 liter/s) AMD spring located in Somerset County, PA. The AMD discharge is the result of runoff that pools behind the low wall of a large former surface coal mine and then travels underground ca. 1 km to emerge at a borehole within the Prince Gallitzin State Forest (40°14'25.25"N, 78°44'49.2"W). This site is especially well suited for studying low-pH Fe(II) oxidation because the discharge flows undiluted by other surface

\* Corresponding author. Mailing address: Department of Civil and Environmental Engineering, The Pennsylvania State University, 212 Sackett Building, University Park, PA 16802-1408. Phone: (814) 863-0578. Fax: (814) 863-7304. E-mail: wdb3@psu.edu.

† Supplemental material for this article may be found at <http://aem.asm.org/>.

∇ Published ahead of print on 19 November 2010.

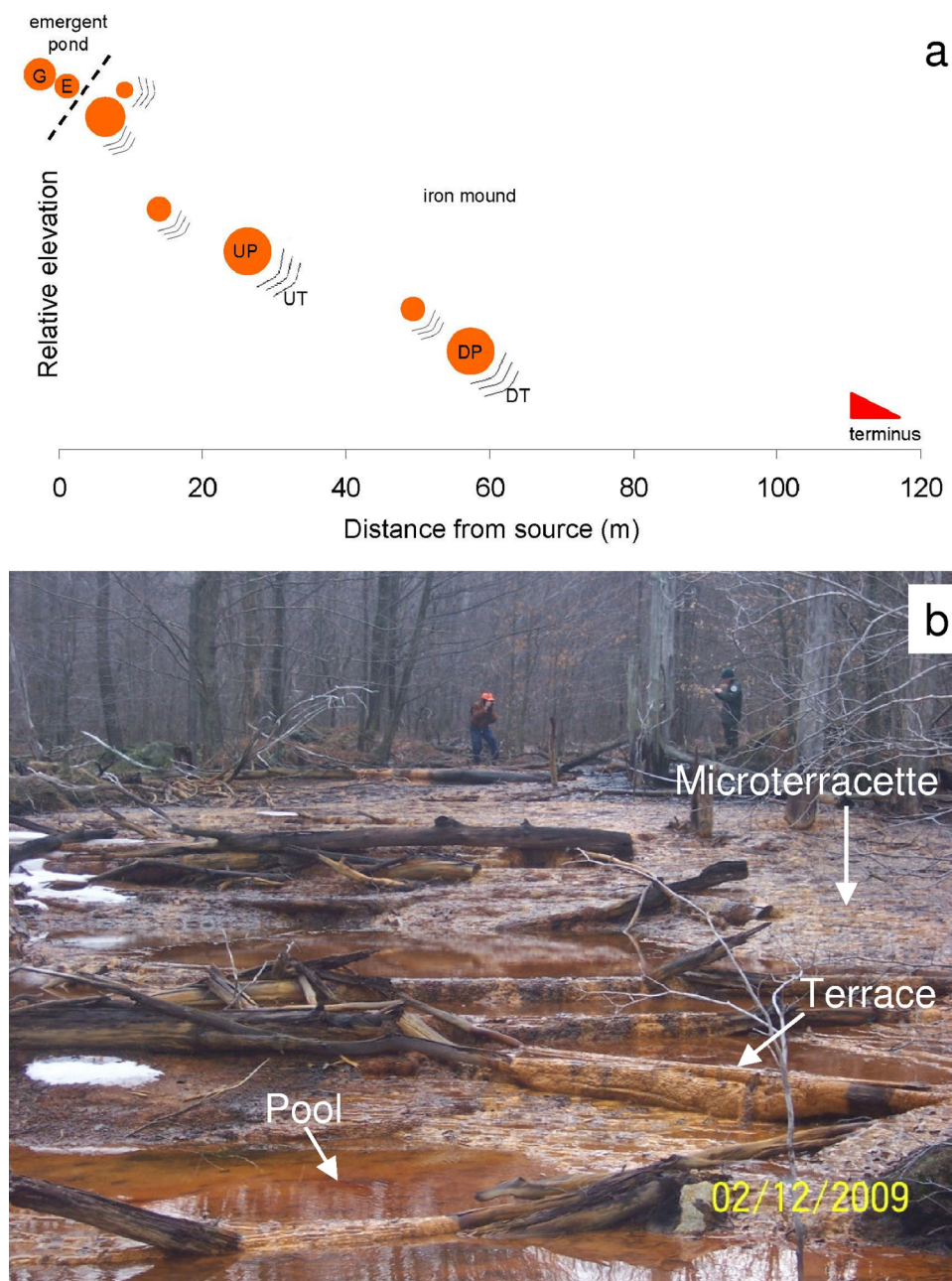


FIG. 1. (a) Site schematic and locations of depositional *facies* identified at the Lower Red Eyes acid mine drainage (AMD) site. Circles represent pools, and series of lines represent terraces. E represents the emergent anoxic AMD spring, and G represents the algae-dominated pond uphill of the spring. UP and UT represent the upstream pool and terrace locations, respectively, while DP and DT represent the downstream pool and terrace locations, respectively. (b) Field photograph showing an uphill view of the Lower Red Eyes iron mound with sequences of pools, terraces, and microterraccettes. The spring (0 m) is located between the two men. The iron mound starts left of the man in the center, where water flows over a large log (7 m downstream). The water flows downhill from point E across the iron mound (i.e., through UP, UT, DP, and DT) to the terminus. The photo was taken approximately 50 m downstream of the spring.

water. After flowing through the forest for nearly 150 m, the discharge seeps back into the ground.

At Lower Red Eyes, 14 sampling sites were selected along a flowpath from the emergent AMD spring (0 m) to 122 m downstream (Fig. 1a). Sampling sites included both terrace and pool depositional *facies* (Fig. 2). Of the 14 sampling sites, an upstream pool (UP), an upstream terrace (UT), a downstream pool (DP), and a downstream terrace (DT) were selected for mineralogical and microbial characterizations and for laboratory reactor studies. The UP and UT locations were selected because they were the first large expanses of distinct

depositional *facies* that allowed for the sampling and removal of several intact pieces of sediments (details below). The UP and UT locations were sampled 27 m and 28 m from the spring, respectively. The DP and DT locations were selected because they were the last paired set of these depositional *facies* before the iron mound transitioned into soft, marshy sediments. The DP and DT sediments were collected 59 and 62 m from the spring, respectively.

Dissolved oxygen (DO), temperature, pH, and conductivity were measured in the field using portable meters as described previously (8). Filtered (0.2- $\mu$ m pore) water samples were preserved in the field to pH < 2 with concentrated HCl

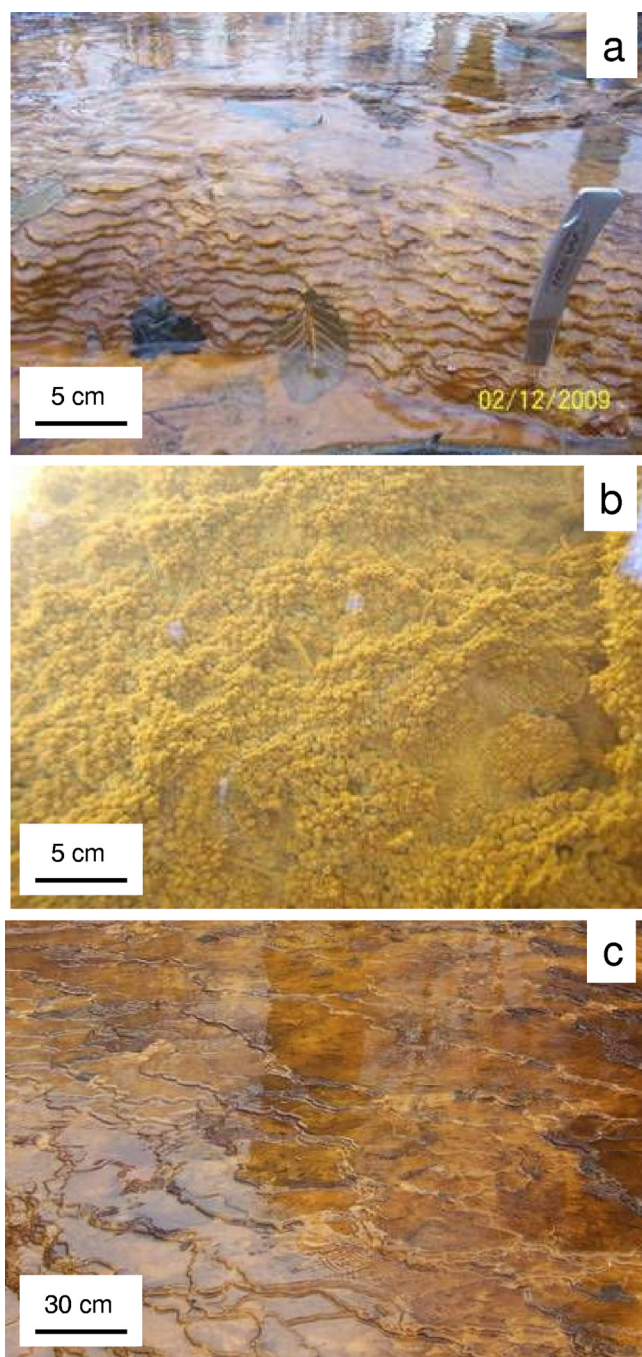


FIG. 2. Field photographs of the characteristic types of depositional facies observed across the Lower Red Eyes iron mound. (a) Terraces were defined as having a vertical drop of  $>5$  cm. (b) Pools (top view) were defined as having a diameter of  $>1.5$  m and a water depth of  $>0.3$  m. (c) Microterraces were defined as having a vertical drop of  $<2$  cm with shallow pools behind and typically extended over several meters in length.

(for dissolved Fe analysis) or concentrated  $\text{HNO}_3$  (for dissolved-metal analysis by inductively coupled plasma-atomic emission spectroscopy [ICP-AES]). Samples for sulfate analysis and cell counts were neither filtered nor acidified. All water samples were transported on ice and stored at  $4^\circ\text{C}$  until analysis.

Sediments for electron microscopy were collected from the top 2 cm and preserved immediately in the field in 2.5% glutaraldehyde. Sediments for X-ray

diffraction (XRD) were not chemically preserved. Sediment and biofilm samples for microbial analyses were collected from the sediment surface with sterile transfer pipettes. Samples for DNA extraction were stored at  $4^\circ\text{C}$  immediately upon collection and transferred to  $-80^\circ\text{C}$  within 4 h. Fluorescent *in situ* hybridization (FISH) samples were preserved immediately in the field in 4% paraformaldehyde (PFA) as described by Macalady et al. (22). Intact pieces of terraces and sediment-covered leaves from the pools were removed with a knife and collected in plastic storage containers for use in flowthrough reactor experiments. All sediment samples were stored at  $4^\circ\text{C}$  until analysis and/or use in laboratory reactors (1 to 12 weeks).

**Mineralogical characterizations.** Unpreserved sediment samples were analyzed for metal oxides and ash content by ICP-AES after lithium metaborate fusion at  $900^\circ\text{C}$ . Samples were prepared for scanning electron microscopy (SEM) as described previously (33) and imaged on an FEI Quanta 200 environmental scanning electron microscope under low vacuum. Higher-magnification images were also collected with a Jeol JSM-6700F field emission scanning electron microscope. XRD patterns were collected by Rigaku D/Max Rapid II XRD with a Mo X-ray tube and a 0.3-mm collimator. Intensities were measured with the omega axis fixed at  $0^\circ$  and phi axis oscillation between  $-20^\circ$  and  $+20^\circ$  with a 10-min exposure time.

**Microbial characterizations.** Acridine orange direct counting (AODC) was used to enumerate cells in both sediment and water samples (16). Cell counts from sediments were performed by extracting 1 g of wet sediment with 9.5 ml of 0.1% sodium pyrophosphate adjusted to pH 3.5 with sulfuric acid. The sodium pyrophosphate solution was pH adjusted to maintain acidic sediment conditions and avoid abiotic Fe(II) oxidation. The sediment-pyrophosphate suspension was shaken at 100 rpm for 30 min and then centrifuged at  $1,000 \times g$  for 10 min. The supernatant extract was diluted ca. 10 to 1,000 times with 0.2- $\mu\text{m}$  filter-sterilized distilled water to bring the microbial counts within the acceptable grid range on the microscope, and then 1 ml of diluted extract was reacted with 1 ml of sterile distilled water and 0.2 ml of acridine orange (AO) stain.

Fluorescence *in situ* hybridization (FISH) analyses were performed as described by Hugenholz et al. (15). Briefly, samples were spotted onto 10-well Teflon-coated slides and, after drying, were dehydrated in 50, 80, and 90% ethanol solutions for 3 min each. Hybridization buffer contained 0.9 M NaCl, 20 mM Tris-HCl at pH 7.4, 0.01% sodium dodecyl sulfate (SDS), 25 ng of fluorescently labeled probe (Table 1), and formamide (concentration varied with probe). After incubation for 2 h at  $46^\circ\text{C}$ , slides were incubated in wash buffer (20 mM Tris-HCl at pH 7.4, 0.01% SDS, and NaCl, based on reference 20) for 15 min at  $48^\circ\text{C}$ . Slides were then rinsed with deionized water and stained with 4',6-diamidino-2-phenylindole (DAPI).

Slides were mounted with Vectashield and viewed with a Nikon Eclipse 80i epifluorescence microscope at  $1,000\times$ . A monochrome Photometrics Coolsnap ES<sup>2</sup> charge-coupled device (CCD) camera was used to obtain photomicrographs with NIS-Elements AS 3.0 software. Population data were generated by counting more than 400 DAPI-stained cells per probe combination. The mean and standard deviation for each FISH probe were calculated directly from counts of multiple photomicrographs. At least eight photos (each representing a different microscope field) were counted from at least two slide wells.

FISH probes used in this study (Table 1) targeted domains as well as broad phylum-level bacterial divisions that are common in AMD environments. We also specifically targeted the genus *Acidithiobacillus*; the genus *Ferroplasma*; and groups I, II, and III of the species *Leptospirillum ferrooxidans*. *Betaproteobacteria*-specific probe Bet42a is known to hit multiple *Gammaproteobacteria* (15, 32). We used the PROBE-MATCH tool in ARB (21) to compare Bet42a against a publicly available database of 23S rRNA sequences (26; <http://www.arb-silva.de>) and found that Bet42a targeted  $>25\%$  of gammaproteobacterial sequences. Here we determined total numbers of *Beta*- and *Gammaproteobacteria* by hybridizing a mixture of Cy3-labeled Gam42a and Bet42a (GAMBET) to each sample and total *Gammaproteobacteria* by hybridizing a separate slide of the same sample with a mixture of Cy3-labeled Gam42a and unlabeled competitor cGam42a. The proportion of total *Betaproteobacteria* was determined by subtracting total Gam42a-labeled cells from total GAMBET-labeled cells. To label the *Ferroplasma* group, we designed probe Ferri643 (Table 1), using the PROBE-DESIGN function in the ARB package (21). Appropriate formamide stringency was determined by using a mixed culture of *Ferroplasma myxofaciens* as a positive control and *Pseudomonas fragi* as a negative control (two mismatches).

DNA extraction and 16S rRNA cloning from upstream pool sediments were performed with bacterial primers 27f and 1492r, as described by Macalady et al. (23). Prior to DNA extraction, iron oxides were removed from sediments by the oxalate washing procedure as described by Senko et al. (28).

**Laboratory reactors.** Water for flowthrough reactors was collected from the AMD emergence, flushed with nitrogen upon returning to the laboratory, stored

TABLE 1. FISH probes used in this study

Probe name <sup>a</sup>	Sequence (5'→3')	% formamide	Specificity	Label	Source or reference
EUB338	GCT GCC TCC CGT AGG AGT	0–50	Most <i>Bacteria</i>	FITC	2
EUB338-II	GCA GCC ACC CGT AGG TGT	0–50	<i>Planctomycetales</i>	FITC	7
EUB338-III	GCT GCC ACC CGT AGG TGT	0–50	<i>Verrucomicrobiales</i>	FITC	7
ARCH915	GTG CTC CCC CGC CAA TTC CT	20	Most <i>Archaea</i>	Cy3	29
THIO1	GCG CTT TCT GGG GTC TGC	35	<i>Acidithiobacillus</i> spp.	Cy3, Cy5	13
LF655	CGC TTC CCT CTC CCA GCC T	35	<i>Leptospirillum ferrooxidans</i> groups I, II, and III	Cy5	4
Ferri643	ACA GAC TCT AGC TTG CCA	35	<i>Ferrovum</i> spp.	Cy3	This study
BET42a	GCC TTC CCA CTT CGT TT	35	Most <i>Betaproteobacteria</i> and some <i>Gammaproteobacteria</i>	Cy3	24
GAM42a	GCC TTC CCA CAT CGT TT	35	Most <i>Gammaproteobacteria</i>	Cy3	24
cGAM42a	GCC TTC CCA CTT CGT TT	35	Competitor for GAM42a	None	24

<sup>a</sup> The mixture of EUB338, EUB338-II, and EUB338-III is also known as EUBMIX, and the mixture of GAM42a and BET42a is also known as GAMBET (see Materials and Methods). GAM42a and BET42a target the 23S rRNA sequence. All other probes target the 16S rRNA sequence.

at 4°C for no more than 1 week, and filtered (0.2 µm) prior to use. Flowthrough reactors were constructed with intact pieces of iron mound sediments placed in two plastic storage containers (13 cm by 8.2 cm by 6.4 cm [length by width by height]) connected in series and open to the atmosphere (see Fig. S1 in the supplemental material). Each reactor contained 175 ml of AMD, corresponding to a 0.6-cm water column height above the sediments. A peristaltic pump was used to pump water from a feed tank into the reactors. The reactor pore volume was defined as the total liquid volume in the two-container reactor series (350 ml). The hydraulic residence time was defined as the time required for one reactor volume to flow through the two containers. Experiments were conducted sequentially at residence times of 10, 5, and 2 h, starting at the longest residence time and finishing at the shortest residence time. Reactors contained either terrace sediments (ca. 100 g, 120 cm<sup>2</sup>) or pool sediments (ca. 12 g, 60 cm<sup>2</sup>) conducted in duplicate reactor series, and single-replicate no-sediment control reactor series were run at the same time. Sediment masses and areas varied because of the nature of the collected sediment pieces. For example, sediment pieces cut from terraces were relatively large, cemented, and thick (ca. 1 to 2 cm), while sediment pieces removed from pools were smaller and loosely deposited as a thin layer (ca. 0.1 to 0.3 cm), typically on an intact leaf (see Fig. S1 in the supplemental material). At the conclusion of experiments conducted with upper terrace and upper pool sediments, the intact sediment reactors were exposed to 50 kGy of <sup>60</sup>Co radiation, and the experiments were repeated.

Water samples were collected at the initial start (time = 0) and after select pore volumes of fluid had been pumped through the reactor series. At the influent and effluent ends of the reactor series, samples were collected and centrifuged at 13,400 rpm for 2 min. Dissolved Fe and Fe(II) were measured from the supernatant. The pH of the supernatant was measured with a semi-micro pH probe. DO was also measured at each sampling point.

**Analytical methods.** Dissolved Fe(II) and dissolved total Fe (after reduction by hydroxylamine-HCl) were determined with the ferrozine assay (30). Dissolved Fe(III) concentrations were determined from the difference between total Fe and Fe(II) measurements. A suite of metal cations, including Al, Co, Fe, Mn, Ni, Si, and Zn, were analyzed by ICP-AES. Sulfate was measured spectrophotometrically by barium sulfate precipitation (Hach method 8051).

**Nucleotide sequence accession numbers.** Nonchimeric 16S rRNA gene sequences have been submitted to GenBank under accession no. HQ420110 to HQ420152.

## RESULTS

**Description of site and definition of facies.** The Lower Red Eyes site can be broadly divided into two distinct geochemical environments. The first environment is the proximal area surrounding the anoxic spring (from 3 m uphill of the spring to 0 m at the spring) and is referred to as the emergent pond depositional facies. The second environment is the iron mound (Fig. 1b) that starts abruptly after the water falls over a 0.5-m-high log (7 m downstream of spring) and the DO increases to near saturation. The Lower Red Eyes iron mound (7 m to

120 m downstream of the spring) was further divided into three distinct depositional facies referred to as (i) terraces consisting of a vertical drop greater than 5 cm (Fig. 2a), (ii) pools of quiescent water with a diameter of 1 to 2 m and a depth of 0.3 to 0.8 m (Fig. 2b), and (iii) microterraces consisting of vertical drops less than 2 cm forming shallow ponds (<2.5 cm deep) behind (Fig. 2c). Our depositional facies were defined based on their cm-scale sediment morphology and are associated with differences in water flow rate, water turbulence, water depth, and terrace height. Based on visual dye tracer studies and volumetric calculations, the hydraulic residence times were estimated to be several hours in the pools, and tens of seconds across the terraces.

In the pool depositional facies, precipitates at Lower Red Eyes displayed a stalked “cauliflower-like” morphology (Fig. 2b). These sediment stalks were somewhat “fluffy” and commonly deposited directly onto leaves and plant debris settled onto the pool bottoms. In contrast, the precipitates on the terraces (Fig. 2a) and across the microterraces (both vertical lips and horizontal bottoms; Fig. 2c) were strongly cemented. These cemented sediments also contained leaves and organic matter.

**Field chemistry.** The Lower Red Eyes spring water emerged with an average pH of 4.0, a DO concentration of <0.3 µM, and dissolved concentrations of 9.7 mM total iron, 9.7 mM Fe(II), 2.1 mM manganese, 1.6 mM aluminum, 0.20 mM zinc, and 31.3 mM sulfate (see Table S1 in the supplemental material). The pH decreased to <2.5, 120 m downstream of the spring (Fig. 3a). DO and temperature increased along the flowpath until DO was nearly saturated and temperature equilibrated according to seasonal conditions (Fig. 3b and c). Dissolved total Fe [sum of Fe(II) and Fe(III)] decreased along the flowpath as a result of Fe(II) oxidation and Fe(III) precipitation (Fig. 3d). While dissolved Fe decreased along the flowpath, the fraction of Fe(III) increased significantly due to Fe(II) oxidation (Fig. 3e). The downstream geochemical trends were similar for all sampling dates, and no seasonal variations were detected.

The relative concentration of dissolved Fe(III) increased downstream, while the relative and absolute concentrations of dissolved Fe(II) decreased as a result of Fe(II) oxidation. Greater than 95% of the dissolved Fe(II) was oxidized to

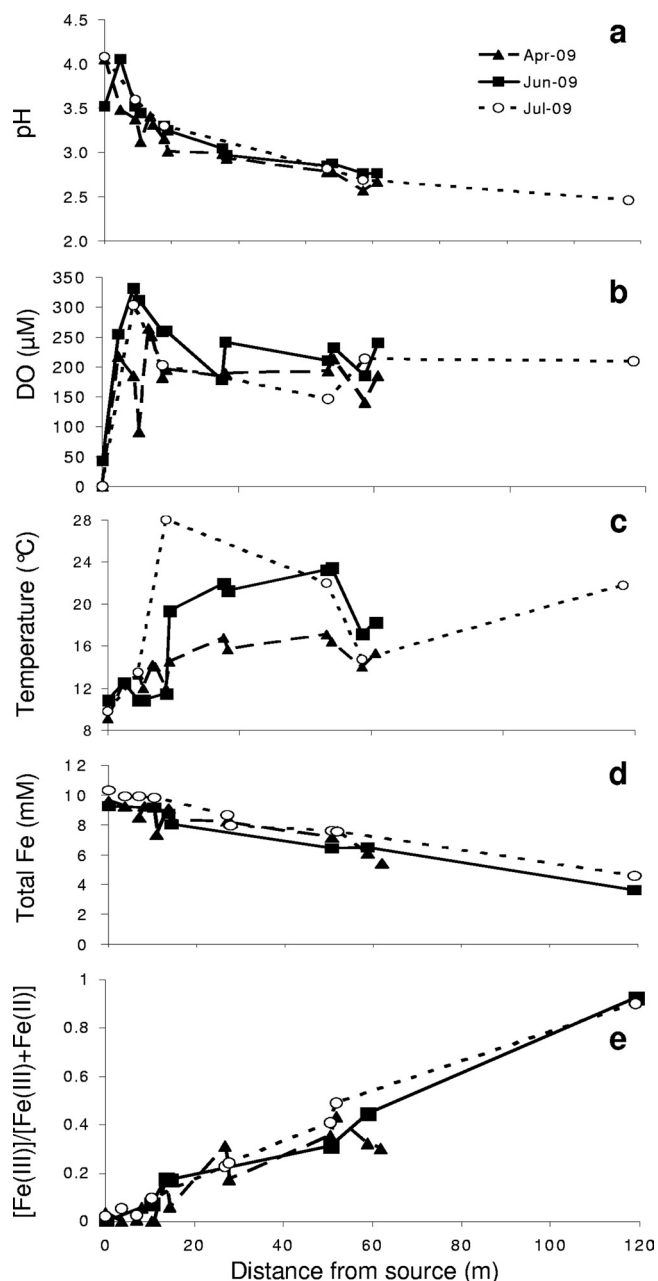


FIG. 3. Water chemistry as function of distance downstream from the Lower Red Eyes AMD spring (located at 0 m). (a) pH, (b) dissolved oxygen (DO), (c) temperature, (d) dissolved total Fe, and (e) ratio of dissolved Fe(III) to dissolved total Fe.

Fe(III) within 120 m of the spring, where the concentration of dissolved Fe(III) increased from  $<1 \mu\text{M}$  at the spring to more than 3 mM 120 m downstream. Within 120 m of the spring, approximately 60% of dissolved total Fe was removed. Although significant removal of dissolved total Fe was observed, no changes in dissolved concentrations of Al, Mn, Zn, Ni, or Co were detected along the flowpath (see Fig. S2 in the supplemental material). The high concentration of protons in these waters (especially at the most downstream locations) effectively outcompeted other metal cations for sorption sites

to the iron oxyhydroxy-sulfate minerals that precipitated from solution, consistent with other studies that have measured trace metal sorption to ferric oxyhydroxides as a function of pH (e.g., see references 1 and 18). In addition, the high concentration of protons in these waters seemed to prevent coprecipitation of the other metal cations into the iron oxyhydroxy-sulfate minerals that created these terraces.

**Mineralogical characterizations.** The metal oxide composition of sediments was determined at four sampling locations within 61 m of the AMD spring. All samples contained predominantly  $\text{Fe}_2\text{O}_3$  ( $\geq 50\%$ ), and organic matter and sulfur that was lost on ignition at  $900^\circ\text{C}$  (30 to 40%) (see Table S2 in the supplemental material). These results were consistent with the field observations of plant matter cemented into the terraces and settled onto the pool bottoms. Considering that no other metals were lost from solution along the flowpath, these results confirmed that there was no selective uptake of trace metals into the Fe precipitates (0.01 to 0.05% m/m oxide detection limits).

XRD indicated that the predominant mineral phase at all sampling sites was poorly crystalline schwertmannite [ $\text{Fe}_8\text{O}_8(\text{OH})_{4.5}(\text{SO}_4)_{1.75}$ ] (see Fig. S3 in the supplemental material), an iron oxyhydroxy-sulfate mineral common in AMD-impacted systems. Minor amounts of goethite were detected at a few sampling points, including the upper terrace and downstream pool locations. Based on SEM images, we found sediment particles occurred as 1- to  $2\text{-}\mu\text{m}$  sized spheroids with a “hedgehog” morphology (see Fig. S4 in the supplemental material) characteristic of schwertmannite (3). Energy-dispersive X-ray spectroscopy (EDS) analysis confirmed a composition of Fe, S, and O. The high signal for S was consistent with XRD and SEM data indicating schwertmannite as the predominant phase. Furthermore, schwertmannite and its crystal morphology were essentially constant across the whole iron mound, regardless of depositional facies.

**Microbial characterizations.** Based on AODC, the water contained low numbers of microbial cells (ca.  $10^4$  cells/ml), while cell counts from the sediments ranged from  $10^6$  to  $10^7$  cells/g. These counts could underestimate biomass concentrations because of cell extraction efficiency and/or AO stain intensity at low pH; however, they are useful for comparison purposes. We used a full-cycle rRNA approach (FISH and 16S rRNA cloning) to describe the microbial community composition of sediments at various distances downstream from the spring (Fig. 4). In preliminary FISH analyses, we found that sediments from the most downstream sites were dominated by *Acidithiobacillus* spp. but that the middle reaches of the iron mound, including the upper pool (UP) sampling location (Fig. 1a), were dominated by rod-shaped *Betaproteobacteria*. In order to further characterize these *Betaproteobacteria*-dominated communities and because the UP location was targeted for reactor experiments, we created a small 16S rRNA clone library from UP sediments. We retrieved 43 nonchimeric, nearly full-length bacterial 16S rRNA gene sequences. The most abundant phylotype ( $>98\%$  sequence similarity) was in the same clade as the iron-oxidizing betaproteobacterium *Ferrovum myxofaciens* (Fig. 5). We subsequently designed FISH probe Ferri643 to target this group (Table 1). The clone library also included multiple clones related to AMD-associated clades in the *Proteobacteria*, eight sequences from the *Acidimi-*

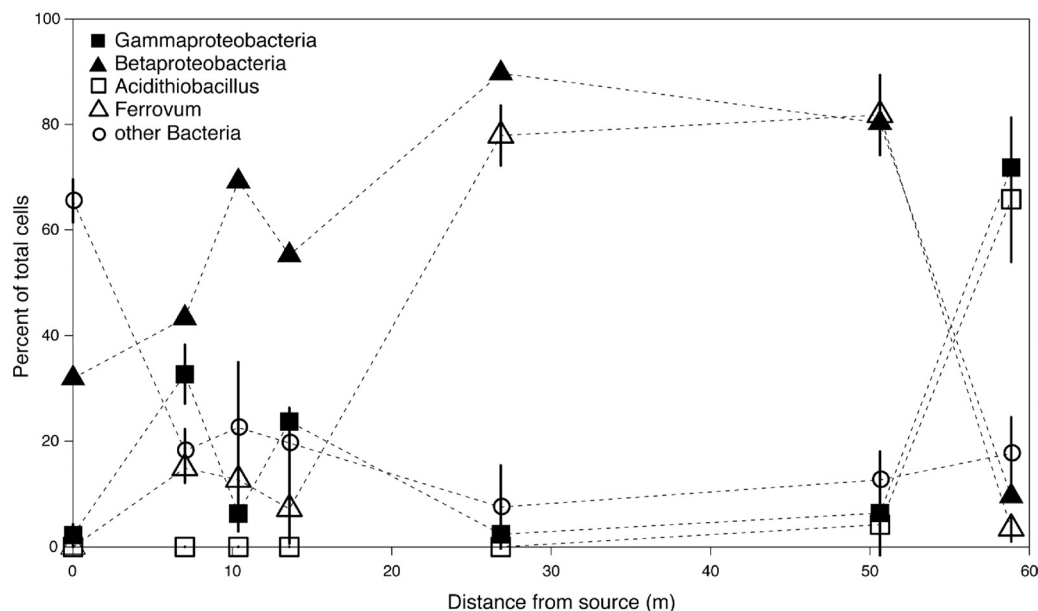


FIG. 4. Changes in Lower Red Eyes microbial communities with downstream distance, based on fluorescence *in situ* hybridization (FISH) of pool sediments. Cell counts are expressed as percentages of total DAPI-stained cells, and error bars represent 1 standard deviation. Corresponding data for all samples are provided in Table S3 in the supplemental material.

*crobiaceae* family (*Actinobacteria*), and two sequences with >98% identity to chloroplasts from *Euglena mutabilis*.

FISH analyses were performed using domain-specific probes to target archaea and bacteria, as well as phylum-level probes to target the *Gamma*- and *Betaproteobacteria* divisions. Both of these divisions contain multiple iron-oxidizing acidophiles that are common in AMD environments (17). At all sites except the emergence, the combination of *Gamma*- and *Betaproteobacteria* probes labeled more than 80% of all DAPI-stained cells. Samples were also probed with LF655 targeting the genus *Leptospirillum* in the *Nitrospira* lineage (groups I, II, and III). *Leptospirillum* cells were detected only in the more acidic samples (e.g., DP and DT, where pH approached 2.5), but accounted for <2% of DAPI-stained cells.

At the anoxic emergence, conspicuous green biofilms were formed by photosynthetic Eukarya, including *Euglena* spp. Elongated cells with rust-colored granules were commonly observed under light microscopy, suggesting Fe sequestration (6). These cells were morphologically similar to *Euglena mutabilis*, which has been identified at many AMD sites (6, 9). Bacterial communities found at the emergence were dominated (>50% total cells) by bacteria with morphologies characteristic of spirochetes. Rod-shaped *Betaproteobacteria* made up 32% of the community. As the water became oxygenated and the pH dropped, *Euglena* decreased in abundance within 7 m of the spring. Also 7 m from the spring, the system abruptly shifted from the emergent pond *facies* to the iron mound.

At 10 m from the spring, *Betaproteobacteria* increased in abundance to 70% of the community. *Ferrovum* appeared as a minor proportion of the community at 10 m from the spring but increased in abundance to over 80% of the community at 52 m from the spring. At 59 m from the spring, *Acidithiobacillus* strains were the dominant microorganisms. More than 65% of all cells were identified as *Acidithiobacillus*, and only 1%

were identified as *Archaea* at this location. No *Acidithiobacillus* cells were observed closer than 28 m to the source. FISH analysis of sediments used for laboratory reactor experiments also reflected the community composition of field sediments, such that *Ferrovum* dominated in upstream sediments and *Acidithiobacillus* dominated in downstream sediments.

Microbial communities were also compared on the basis of depositional *facies*. Overall, microbial communities from adjacent pools and terraces were similar. Changes in microbial community composition were more dependent upon distance from the emergence (Fig. 4) than the depositional environment. However, this conclusion is based on FISH analyses targeting only broad microbial divisions and three specific genera, and so a different technique such as 16S rRNA cloning might resolve differences in community composition that we did not detect here. Furthermore, we did detect some differences between pool and terrace microbial communities: for example, *Euglena* strains were extremely rare in terrace sediments (see Table S3 in the supplemental material).

**Low-pH Fe(II) oxidation in laboratory reactors.** The rate and extent of Fe(II) oxidation were measured to determine whether biogeochemical kinetics changed as a function of depositional *facies* (Table 2). Results for the upstream terrace sediments operated at a 10-h residence time are presented in Fig. 6. Within 2 pore volumes, the dissolved Fe(II) concentration decreased from 9.8 mM to nearly 4.5 mM, and the reactor reached a pseudo-steady-state condition with respect to the effluent Fe(II) concentration. The concentration of dissolved Fe also decreased from 9.8 mM to below 8 mM, indicative of Fe(III) precipitation. The pH dropped rapidly over time, from pH 4.5 to pH 2.7 within 2 pore volumes. There was significantly less effluent DO in the “live” sediment reactor (34  $\mu$ M) than in the sterilized sediment reactors and no-sediment control reactors (both  $\sim$ 250  $\mu$ M). The consumption of Fe(II) and DO, the

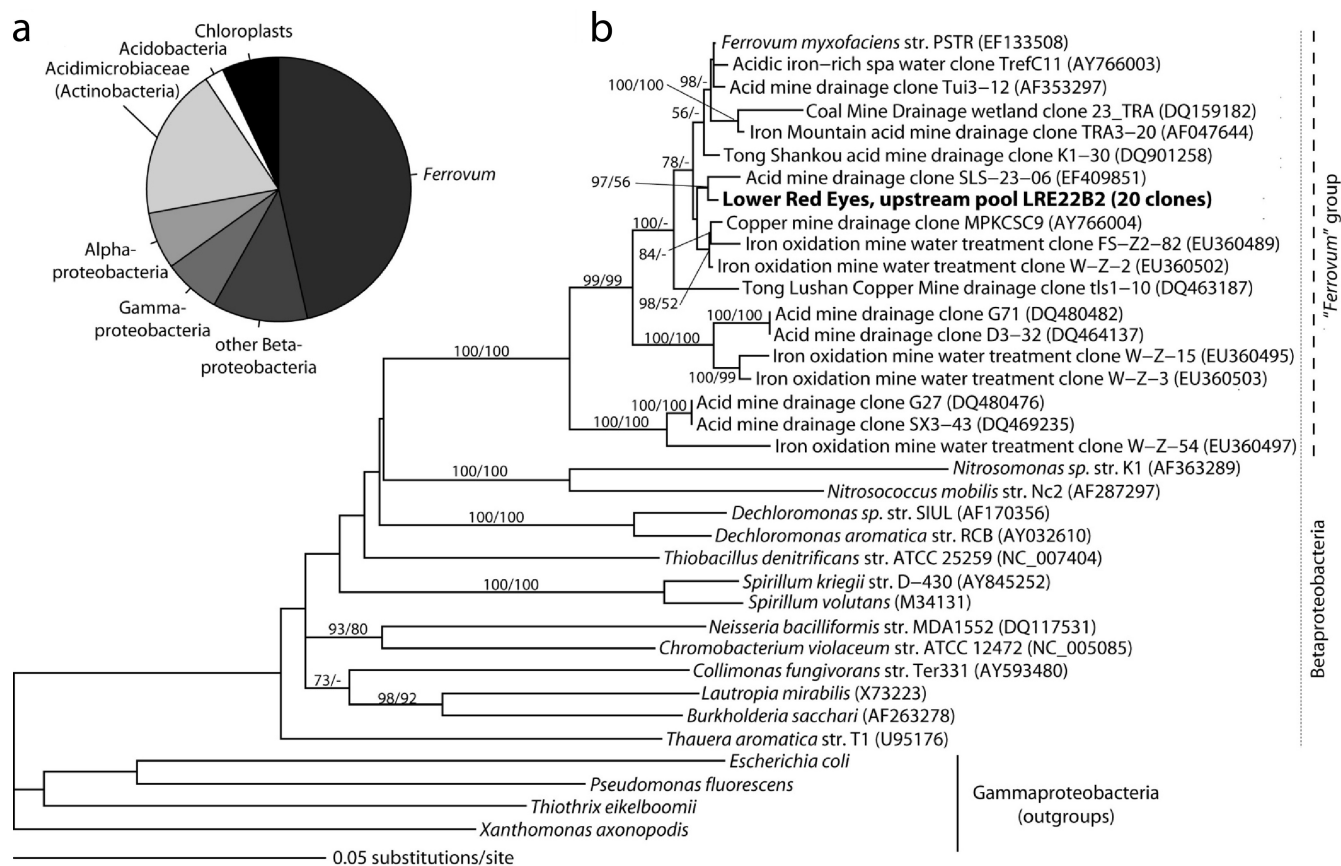


FIG. 5. (a) Phylum-level distribution of 16S rRNA sequences obtained from the upstream pool sediments (27 m downstream of the Lower Red Eyes spring). (b) Maximum-likelihood tree showing the phylogenetic relationship of the most common clone obtained from these sediments related to *Betaproteobacteria* sequences. Bootstrap values for nodes greater than 50% support, determined with 1,000 replicates, are displayed as percentages. GenBank accession numbers are in parentheses. Scale bars represent 0.05 substitution per nucleotide site.

drop in pH and total dissolved Fe, and the contrasting behavior between the “live” sediments and the control reactors were all consistent with biological Fe(II) oxidation followed by hydrolysis and precipitation of Fe(III). These geochemical changes were also consistent with gradients observed with distance downstream from the Lower Red Eyes spring (Fig. 3).

To compare results over these experiments in which we

incrementally decreased the hydraulic residence time and to compare results between the different sediments, we present normalized dissolved concentration ratios of  $[Fe(II)]_{out}/[Fe(II)]_{in}$  to account for any variances. With all of the sediments tested, the  $[Fe(II)]_{out}/[Fe(II)]_{in}$  ratios increased as the hydraulic residence time decreased (Fig. 7). These data suggest that the hydraulic residence across a natural or engineered iron

TABLE 2. Summary of Fe(II) oxidation rates ( $R_{Fe(II)}$ ) measured from laboratory reactors with sediments collected from the Lower Red Eyes acid mine drainage site<sup>a</sup>

Parameter	Result for location:			
	Upstream		Downstream	
	Terrace	Pool	Terrace	Pool
Avg mass of sediments (g)	103 ± 9.30	13.0 ± 9.70	100 ± 3.20	11.8 ± 2.58
Avg surface area of sediments (cm <sup>2</sup> )	130 ± 17.0	59.8 ± 11.2	119 ± 17.9	56.5 ± 17.5
Avg net $Fe(II)_{out}/Fe(II)_{in}$	0.45 ± 0.04	0.61 ± 0.02	0.73 ± 0.02	0.80 ± 0.01
Avg net $Fe_{out}/Fe_{in}$	0.73 ± 0.02	0.79 ± 0.09	0.86 ± 0.04	0.88 ± 0.02
$R_{Fe(II)}$ ( $10^{-7}$ mol liter <sup>-1</sup> s <sup>-1</sup> )	1.58 ± 0.53	1.03 ± 0.31	0.75 ± 0.25	0.57 ± 0.23
$R_{Fe(II)}$ ( $10^{-9}$ mol liter <sup>-1</sup> s <sup>-1</sup> g <sup>-1</sup> )	1.60 ± 0.41	10.4 ± 6.58	0.74 ± 0.24	4.79 ± 1.58
$R_{Fe(II)}$ ( $10^{-9}$ mol liter <sup>-1</sup> s <sup>-1</sup> cm <sup>-2</sup> )	1.25 ± 0.49	1.75 ± 0.56	0.63 ± 0.17	1.08 ± 0.52

<sup>a</sup> All results were calculated from dissolved Fe(II) and dissolved total Fe concentrations measured under pseudo-steady-state conditions achieved at a 10-h hydraulic residence time. Sediment mass and surface area values represent means ± standard deviations (SD) for four measurements (where  $n = 4 =$  duplicates from two reactor series = 4 sediment pieces). Rate ( $R$ ) and extent values represent means ± SD calculated from multiple measurements made under the pseudo-steady-state conditions (3 to 5 sampling points) using duplicate reactor series (where  $n = 6$  to  $10 = 3$  to 5 sampling points × 2 duplicate reactor series).

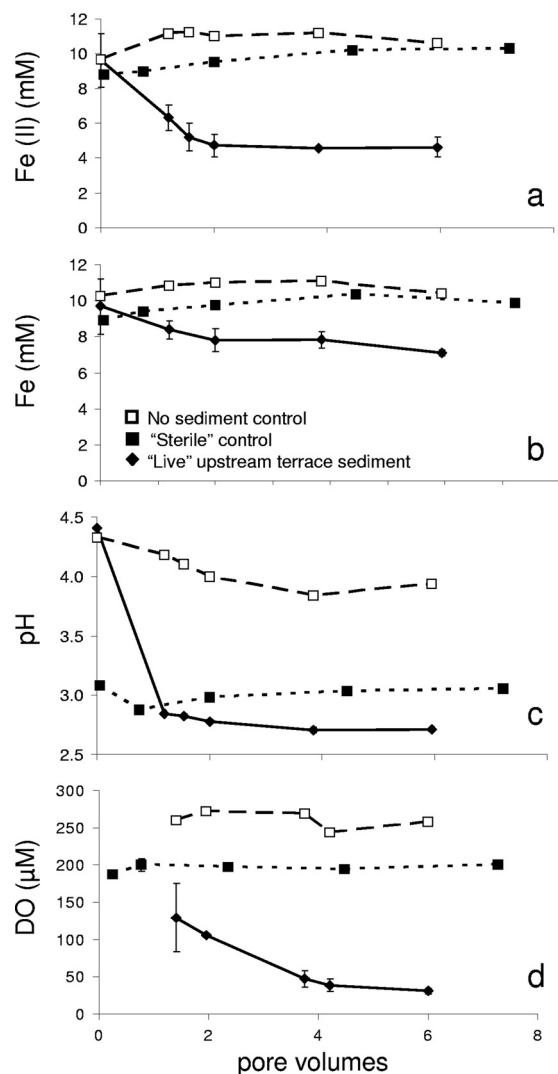


FIG. 6. Results from laboratory experiments conducted with intact sediment pieces removed from the upstream terrace. Experiments were conducted such that 1 pore volume of fluid was pumped through the reactor series every 10 h. (a) The extent of Fe(II) oxidation achieved a pseudo-steady-state condition after 2 pore volumes of operation. (b to d) Dissolved total Fe (b), pH (c), and dissolved oxygen (DO) (d) as a function of time.

mound utilized for low pH Fe(II) oxidation will exert significant control on treatment performance. Compared to sediments collected from the upstream locations, the sediments collected from the downstream locations had higher  $[\text{Fe(II)}]_{\text{out}}/[\text{Fe(II)}]_{\text{in}}$  ratios. For example, at the 10-h residence time, the  $[\text{Fe(II)}]_{\text{out}}/[\text{Fe(II)}]_{\text{in}}$  ratio for the upstream terrace sediments was 0.45, while the  $[\text{Fe(II)}]_{\text{out}}/[\text{Fe(II)}]_{\text{in}}$  ratio for the downstream terrace sediments was 0.72 (Fig. 7). These experiments were all conducted with nearly identical influent water chemistries, and abiotic oxidation of Fe(II) was negligible. Therefore, we speculate that these differences were caused by differences in the microbial communities found at these locations (i.e., *Ferrovum* dominated in upstream sediments and *Acidithiobacillus* dominated in downstream sediments).

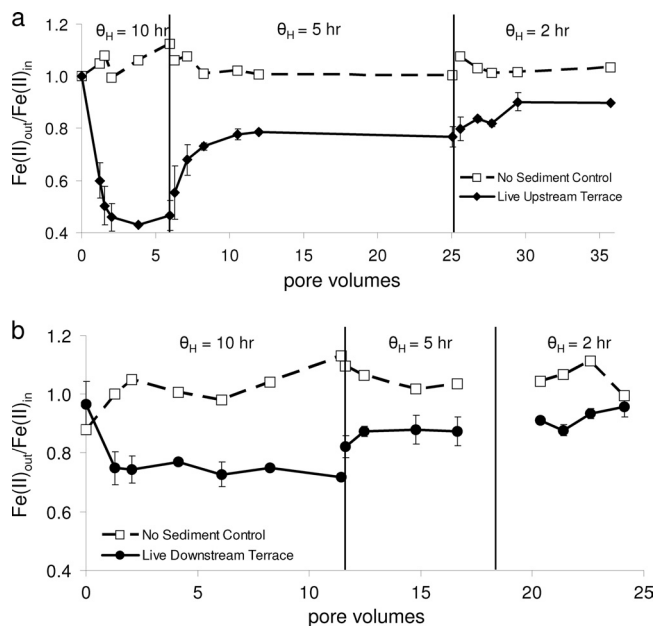


FIG. 7. Results from laboratory experiments conducted with upstream terrace sediments (a) and downstream terrace sediments (b). Experiments began at a 10-h residence time ( $\theta_H =$  time to convey 1 pore volume) that was incrementally reduced to 5 h and 2 h (delineated with vertical lines). For these normalized results, influent dissolved Fe(II) concentrations ranged from 9.7 to 10.9 mM in panel a and from 9.4 to 10.3 mM in panel b.

## DISCUSSION

Based on the rates of Fe(II) oxidation measured (at pseudo-steady state) in the laboratory reactors (Table 2), we found that these sediments could be quite effective for AMD treatment. All measured rates  $[0.57 \times 10^{-7}$  to  $1.58 \times 10^{-7}$  mol Fe(II) liter $^{-1}$  s $^{-1}$ ] were within 1 order of magnitude of rates reported by Kirby and Brady (19) and Nordstrom (25). Surface area-normalized rates are commonly used in the design of AMD treatment systems in which performance, reported in terms of grams of metal removed per day per square meter, is used for sizing ponds and wetlands. We measured surface area-normalized rates of 3.4 to 6.3 g Fe day $^{-1}$  m $^{-2}$  for all sediments tested. In comparison, design guidelines for iron removal from net acid coal mine drainage using aerobic wetlands range from 2 to 5 g Fe day $^{-1}$  m $^{-2}$  (14). We also found that Fe(II) oxidation was strongly dependent on the overlying water height (0.6, 2, or 3 cm), in which greater Fe(II) oxidation occurred in shallower water (data not shown). Therefore, in addition to the microbial community (Fig. 4) and the hydraulic residence time (Fig. 7), the hydrodynamic conditions (e.g., sheet flow and turbulence) will impact Fe(II) oxidation rates and treatment system performance.

Studies of extreme acid mine drainage environments such as Iron Mountain, CA (5), and the Rio Tinto (12) indicate that *Leptospirillum* populations are often important in very low-pH AMD niches (e.g., pH < 2), where they apparently outcompete *Acidithiobacillus* species with similar Fe(II) oxidation metabolisms. At Lower Red Eyes, *Leptospirillum* populations were detected in the most distal, low-pH sample sites but comprised less than 2% of the total cells. This is perhaps not surprising

since the lowest pH measured at the bottom of the Lower Red Eyes iron mound was pH 2.4. It is possible that factors other than pH will prove to play a role in mediating competition between *Leptospirillum* and *Acidithiobacillus* populations in AMD. However, our results are consistent with previous studies in which *Leptospirillum* populations are minor or absent in AMD environments above pH 2.5 (31).

This research was motivated by work conducted in travertine-depositing hot spring systems (10, 11), and in hopes of identifying a unique depositional *facies* in iron-depositing “cold” spring systems that could be exploited for the remediation of AMD. In the work conducted at Angel Terrace, YNP, depositional *facies* were defined based on sediment petrography and directly correlated with distance from the spring. In other words, the identified depositional *facies* transitioned from one into another as a function of downstream distance, and this coincided with the major physical and geochemical gradients across the terrace. In contrast, we identified depositional *facies* distributed across the whole iron mound, irrespective of downstream distance and, therefore, not linked to the evolving geochemical conditions along the water flowpath.

With this clarification in mind, our results are consistent with the Angel Terrace work in which we found distinctly different microbial communities as a function of distance downstream of the emergent spring. However, our results contrast with the Angel Terrace work because, for paired sets of pool and terrace depositional *facies* located close together (1 to 3 m apart), we found only minor differences in the microbial communities. For this iron-depositing system, we also found no correlation between depositional *facies* and the predominant mineral phase (all schwertmannite) or its crystal morphology (all “hedgehog” spheroids).

The present study allows us to conclude with certainty that depositional *facies* are not the major determinant of microbial community structure in this system. However, FISH data did document substantial transitions between microbial communities along downstream flowpaths (Fig. 4), including a major transition between the emergence and 10 m downstream and another transition between 50 and 60 m downstream. Geochemical, physical, and/or hydrodynamic conditions that change along downstream flowpaths, but do not strongly affect depositional *facies*, therefore, likely exert significant control on microbial spatial distributions. Downstream gradients are especially steep for pH, redox potential, temperature, and iron speciation. With our current data set, we were unable to deconvolute the effects of these parameters that covary along the flowpath and, therefore, cannot speculate further about which factors are most important. Work currently in progress will allow us to address hypotheses about which parameters define the ecological niches of *Acidithiobacillus*, *Ferrovum*, and other iron-oxidizing and phototrophic microbial populations important at Lower Red Eyes and similar AMD sites.

#### ACKNOWLEDGMENTS

This work was supported by the National Science Foundation under grant no. CHE-0431328 and by the Pennsylvania Department of Environmental Protection, Bureau of Abandoned Mine Reclamation.

We thank Brent Means from the U.S. Office of Surface Mining and Malcolm Crittenden from the Pennsylvania Department of Environmental Protection for directing us to the Lower Red Eyes site. We

thank D. Barrie Johnson from the University of Wales for providing *Ferrovum myxofaciens* for the development of our FISH probe.

#### REFERENCES

- Ainsworth, C. C., J. L. Polin, P. L. Gassman, and W. G. Van Der Sluys. 1994. Cobalt, cadmium, and lead sorption to hydrous iron oxide: residence time effect. *Soil Sci. Soc. Am. J.* **58**:1615–1623.
- Amann, R., et al. 1990. Combination of 16S rRNA-targeted oligonucleotide probes with flow cytometry for analyzing mixed microbial populations. *Appl. Environ. Microbiol.* **56**:1919–1925.
- Bigam, J. M., U. Schwertmann, L. Carlson, and E. Murad. 1990. A poorly crystallized oxyhydroxysulfate of iron formed by bacterial oxidation of Fe(II) in acid mine waters. *Geochim. Cosmochim. Acta* **54**:2743–2758.
- Bond, P. L., and J. F. Banfield. 2001. Design and performance of rRNA targeted oligonucleotide probes for in situ detection and phylogenetic identification of microorganisms inhabiting acid mine drainage environments. *Microb. Ecol.* **41**:149–161.
- Bond, P. L., G. K. Druschel, and J. F. Banfield. 2000. Comparison of acid mine drainage microbial communities in physically and geochemically distinct ecosystems. *Appl. Environ. Microbiol.* **66**:4962–4971.
- Brake, S. S., H. K. Dannelly, K. A. Connors, and S. T. Hasiotis. 2001. Influence of water chemistry on the distribution of an acidophilic protozoan in an acid mine drainage system at the abandoned Green Valley coal mine, Indiana, U.S.A. *Appl. Geochem.* **16**:1641–1652.
- Daims, H., A. Brühl, R. Amann, K.-H. Schleifer, and M. Wagner. 1999. The domain-specific probe EUB338 is insufficient for the detection of all Bacteria: development and evaluation of a more comprehensive probe set. *Syst. Appl. Microbiol.* **22**:434–444.
- DeSa, T. C., J. F. Brown, and W. D. Burgos. 2010. Laboratory and field-scale evaluation of low-pH Fe(II) oxidation at Hughes Borehole, Portage, Pennsylvania. *Mine Water Environ.* **16**:237–247.
- España, J. S., E. S. Pastor, and E. L. Pamo. 2007. Iron terraces in acid mine drainage systems: a discussion about the organic and inorganic factors involved in their formation through observations from the Tintillo acidic river (Riotinto mine, Huelva, Spain). *Geosphere* **3**:133–151.
- Fouke, B. W., et al. 2000. Depositional *facies* and aqueous-solid geochemistry of travertine-depositing hot springs (Angel Terrace, Mammoth Hot Springs, Yellowstone National Park, U.S.A.). *J. Sediment Res.* **70**:565–585.
- Fouke, B. W., G. T. Bonheyo, B. Sanzenbacher, and J. Frias-Lopez. 2003. Partitioning of bacterial communities between travertine depositional *facies* at Mammoth Hot Springs, Yellowstone National Park, U.S.A. *Can. J. Earth Sci.* **40**:1531–1548.
- García-Moyano, A., E. González-Toril, M. Moreno-Paz, V. Parro, and R. Amils. 2008. Evaluation of *Leptospirillum* spp. in the Río Tinto, a model of interest to bihydrometallurgy. *Hydrometallurgy* **94**:155–161.
- González-Toril, E., E. Llobet-Brossa, E. O. Casamayor, R. Amann, and R. Amils. 2003. Microbial ecology of an extreme acidic environment, the Tinto River. *Appl. Environ. Microbiol.* **69**:4853–4865.
- Hedin, R. S., and R. W. Nairn. 1992. Designing and sizing passive mine drainage treatment systems. Proceedings of the 13th Annual WV Surface Mine Drainage Task Force Symposium. <http://wvmdtaskforce.com/proceedings/1992.cfm>. Accessed 18 January 2010.
- Hugenholtz, P., G. W. Tyson, and L. L. Blackall. 2001. Design and evaluation of 16S rRNA-targeted oligonucleotide probes for fluorescent in situ hybridization, p. 29–42. *In* M. Aquino de Muro and R. Rapley (ed.), *Gene probes: principles and protocols*. Humana Press, London, United Kingdom.
- Hurst, C. J., R. L. Crawford, M. J. McInerney, G. R. Knudsen, and L. D. Stetzenbach (ed.). 2002. *Manual of environmental microbiology*, 2nd ed., p. 511. ASM Press, Washington, DC.
- Johnson, D. B., and K. B. Hallberg. 2003. The microbiology of acidic mine waters. *Res. Microbiol.* **154**:466–473.
- Kinniburgh, D. G., and M. L. Jackson. 1982. Concentration and pH dependence of calcium and zinc adsorption by iron hydrous oxide gel. *Soil Sci. Soc. Am. J.* **46**:56–61.
- Kirby, C. S., and J. A. Elder Brady. 1998. Field determination of Fe<sup>2+</sup> oxidation rates in acid mine drainage using a continuously-stirred tank reactor. *Appl. Geochem.* **13**:509–520.
- Lathe, R. 1985. Synthetic oligonucleotide probes deduced from amino acid sequence data: theoretical and practical considerations. *J. Mol. Biol.* **183**:1–12.
- Ludwig, W., et al. 2004. ARB: a software environment for sequence data. *Nucleic Acids Res.* **32**:1363–1371.
- Macalady, J. L., D. S. Jones, and E. H. Lyon. 2007. Extremely acidic, pendulous microbial biofilms from the Frasassi cave system, Italy. *Environ. Microbiol.* **9**:1402–1414.
- Macalady, J. L., et al. 2008. Niche differentiation among sulfur-oxidizing bacterial populations in cave waters. *Int. Soc. Microb. Ecol. J.* **2**:509–601.
- Manz, W., R. Amann, W. Ludwig, M. Wagner, and K.-H. Schleifer. 1992. Phylogenetic oligodeoxynucleotide probes for the major subclasses of Proteobacteria: problems and solutions. *Syst. Appl. Microbiol.* **15**:593–600.
- Nordstrom, D. K. 1985. The rate of ferrous iron oxidation in a stream

- receiving acid mine effluent. U.S. Geol. Surv. Water-Supply Pap. **2270**:113–119.
26. **Pruesse, E., et al.** 2007. SILVA: a comprehensive online resource for quality checked and aligned ribosomal RNA sequence data compatible with ARB. *Nucleic Acids Res.* **35**:7188–7196.
  27. **Reading, H. G.** 1996. *Sedimentary environments: processes, facies, and stratigraphy*. Blackwell Science, London, United Kingdom.
  28. **Senko, J. M., P. Wanjugi, M. Lucas, M. A. Bruns, and W. D. Burgos.** 2008. Characterization of Fe(II) oxidizing bacterial activities and communities at two acidic Appalachian coalmine drainage-impacted sites. *Int. Soc. Microb. Ecol. J.* **2**:1134–1145.
  29. **Stahl, D. A., and R. Amann.** 1991. Development and application of nucleic acid probes, p. 205–248. *In* E. Stackebrandt and M. Goodfellow (ed.), *Nucleic acid techniques in bacterial systematics*. John Wiley & Sons, Ltd., Chichester, England.
  30. **Stookey, L. L.** 1970. Ferrozine—a new spectrophotometric reagent for iron. *Anal. Chem.* **42**:779–781.
  31. **Tan, G.-L., et al.** 2009. Seasonal and spatial variations in microbial community structure and diversity in the acid stream draining across an ongoing surface mining site. *FEMS Microbiol. Ecol.* **70**:277–285.
  32. **Yeates, C., A. M. Saunders, G. R. Crocetti, and L. L. Blackall.** 2003. Limitations of the widely used GAM42a and BET42a probes targeting bacteria in the *Gammaproteobacteria* radiation. *Microbiology* **149**:1239–1247.
  33. **Zhang, G., H. Dong, J. Kim, and D. D. Eberl.** 2007. Microbial reduction of structural Fe<sup>3+</sup> in nontronite by a thermophilic bacterium and its role in promoting the smectite to illite reaction. *Am. Mineral.* **92**:1411–1419.